

Deep-UV photoemission electron microscopy for imaging nanoscale heterogeneity and defects in gallium nitride

Andrew Winchester^{a,b}, Michael Mastro^c, Travis Anderson^c, Jennifer Hite^c, Andrei Kolmakov^a,
Sujitra Pookpanratana^{*a}

^aNanoscale Device Characterization Division, National Institute of Standards and Technology, Gaithersburg, MD; ^bInstitute for Soft Matter, Georgetown University, Washington, DC, ^cU.S. Naval Research Laboratory, Washington, DC

ABSTRACT

Gallium nitride (GaN) is a promising wide-bandgap material for high-power electronics, where GaN-on-GaN homoepitaxy is being developed for fabrication of compact high-voltage vertical devices. However, variation in GaN substrate quality strongly influences the properties of epitaxial layers grown on top, which in turn affects device performance and reliability. Hence, better knowledge of the surface electronic properties is needed, especially after wafer processing steps that can introduce surface contaminants and oxide layers. Photoemission-based techniques provide chemical and electronic information but are surface-sensitive; therefore, the formation of native oxides or contamination from ambient conditions can affect findings. Here, we present the initial results of various surface treatment methods on the electronic properties of p-type GaN epitaxial layers grown via metal-organic chemical vapor deposition (MOCVD) in preparation for photoemission electron spectroscopy and microscopy characterization. We use X-ray photoelectron spectroscopy (XPS) to evaluate changes in residual contamination after treatment. We find that piranha-based cleaning methods have large reductions in surface carbon contamination, while NH_4OH and HCl -based treatments remove surface oxide. The elemental core levels and valence band correspondingly exhibit binding energy shifts with the different treatment methods, indicating reduced surface band-bending. Both XPS and initial photoemission electron microscopy results of the photoelectron yield suggest a deeper valence band edge location with respect to the Fermi energy measured for the forming gas plasma-cleaned sample. These results demonstrate that combined ex-situ treatments for carbon and oxygen removal are more effective, yet further in-situ cleaning is necessary for more complete contaminant removal.

Keywords: gallium nitride, GaN on GaN, pn GaN, surface cleaning, photoelectron spectroscopy, photoemission electron microscopy

*sujitra@nist.gov

1. INTRODUCTION

In recent years, modernization of the electric grid, as well as electrification of automotive technologies, has led to increasing demands on high-power electronics¹. In order to meet these demands, next-generation high-power devices are currently being researched and developed, with wide-bandgap semiconductors, such as gallium nitride (GaN), poised to overtake traditional silicon power devices in terms of performance and device footprint^{2,3}. Lateral GaN high electron mobility transistors (HEMTs) and silicon carbide metal-oxide-semiconductor field-effect transistors (MOSFETs) have already achieved market success⁴⁻⁶; however, scalable high-power devices require vertical structures to fully utilize the properties of GaN^{3,7,8}. While kV-class power devices have been demonstrated for vertical GaN archetypes, the fabrication technologies for full commercial production are not yet mature^{2,3,7,8}. This is due to several material and engineering issues which must be overcome to realize reliable, reproducible, and high-performance devices.

One of the main issues has been to develop GaN on GaN growth, i.e., growing controlled GaN epitaxial layers on a GaN substrate for vertical device structures^{3,7,8}. Early commercial GaN substrates suffered from a large density of dislocations, which was reduced via patterned growth substrates to aggregate dislocations⁹ and can be further reduced using different growth methods¹⁰. Elimination of dislocations is crucial for device reliability, as dislocations in the substrate are known to propagate through the epitaxial growth, compromising the active device layers^{11,12}. For example, substrates with patterned arrays of dislocation centers exhibit spatially-varying device performance and failure locations¹³⁻¹⁷. However, direct correlation between defective substrate areas, dislocations, and device performance is not straightforward: certain defects appear to be more harmful for devices than others^{11,12,16,17}. Therefore, knowledge of the electronic properties of these defects, which propagate to the surface during the epitaxial growth, is needed to understand the device failure pathways.

Photoelectron spectroscopy can give detailed information about electronic and chemical states at a material surface. However, photoelectron spectroscopy is surface-sensitive due to the short inelastic mean free path of electrons, meaning that formation of native oxides or contaminants from air exposure can affect interpretation of results. Hence, GaN surface preparation is crucial for obtaining reliable results, and importantly, surface cleanliness and preparation is critical for fabrication of GaN devices. For example, contaminants such as carbon and silicon at growth interfaces can dramatically affect device performance¹⁸⁻²⁰. Unsurprisingly, surface preparation of GaN has been a long and ongoing research topic²¹⁻²⁶.

As part of our goal to reliably measure the surface electronic properties of GaN, here we report on ex-situ cleaning of p-type GaN epitaxial layers using several commonly available methods. We quantify the changes in surface contamination using X-ray photoelectron spectroscopy (XPS) for the different cleaning methods, and find that a combination of methods (e.g., piranha + NH₄OH and piranha + HCl) works better for removing both carbon and oxygen from the GaN surface. After treatments with piranha and HCl, sulfate and metal chloride are also observed, respectively. Further, we find that ex-situ plasma cleaning in a forming gas mixture removes carbon contamination; however, it also causes a large shift in the core level binding energies, opposite to that induced by the chemical treatments, indicating a more n-type surface. Initial photoemission electron microscopy (PEEM) measurements confirm the changes in the valence band position for the plasma-treated sample.

2. METHODOLOGY

2.1 GaN samples

The GaN samples investigated were 500 nm thick p-type (Mg dopant) layers epitaxially grown via metal-organic chemical vapor deposition (MOCVD) on an 8 μm thick unintentionally doped (UID) buffer layer on an n-type GaN substrate^{16,17}. The samples were coated in photoresist for transport. A 1 cm² wafer piece was cleaved into four roughly equal sized pieces, as illustrated in the top row of Figure 1. The cleaved pieces were then cleaned via the different methods described in section 2.2.

2.2 GaN cleaning procedures

The photoresist was removed from all GaN samples by sonication in acetone for 5 min, followed by sonication in isopropanol (IPA) for 5 min, then dried with nitrogen. One piece of GaN was initially kept aside as a reference sample (Ref.) for comparison to treatments. The overall cleaning and measurement flow is illustrated in Figure 1 and the specific treatment details are listed in Table 1.

Table 1. Parameters for the various cleaning procedures.

Sample	First Treatment	Second Treatment
Reference	-	-
NH ₄ OH	NH ₄ OH (15 mol L ⁻¹), 15 min	-
Piranha	H ₂ SO ₄ (18 mol L ⁻¹) and H ₂ O ₂ (9.8 mol L ⁻¹), H ₂ O ₂ volume fraction is 0.25, 15 min	-
Piranha + NH ₄ OH	H ₂ SO ₄ (18 mol L ⁻¹) and H ₂ O ₂ (9.8 mol L ⁻¹), H ₂ O ₂ volume fraction is 0.25, 15 min	NH ₄ OH (15 mol L ⁻¹), 15 min
HCl	HCl (9.45 mol L ⁻¹), 3 min	-
Piranha + HCl	H ₂ SO ₄ (18 mol L ⁻¹) and H ₂ O ₂ (9.8 mol L ⁻¹), H ₂ O ₂ volume fraction is 0.25, 15 min	HCl (9.45 mol L ⁻¹), 3 min
HCl + Plasma (previously HCl only)	HCl (9.45 mol L ⁻¹), 4 min	N ₂ /H ₂ plasma, N ₂ volume fraction is 0.95, 773 K, 30 min

All samples were rinsed with deionized (DI) water and blown dry with N₂ after chemical treatment. Samples were immediately transported and loaded into the XPS vacuum chamber within 30 min after treatment.

Plasma cleaning was performed in a quartz tube furnace and the sample was placed approximately 1 cm downstream from the plasma plume during treatment. The plasma conditions were 20 W power, 53 kPa pressure, and a 10 cm³ min⁻¹ flow rate. The sample was transported in a N₂-filled glovebag and immediately loaded into the XPS after plasma treatment.

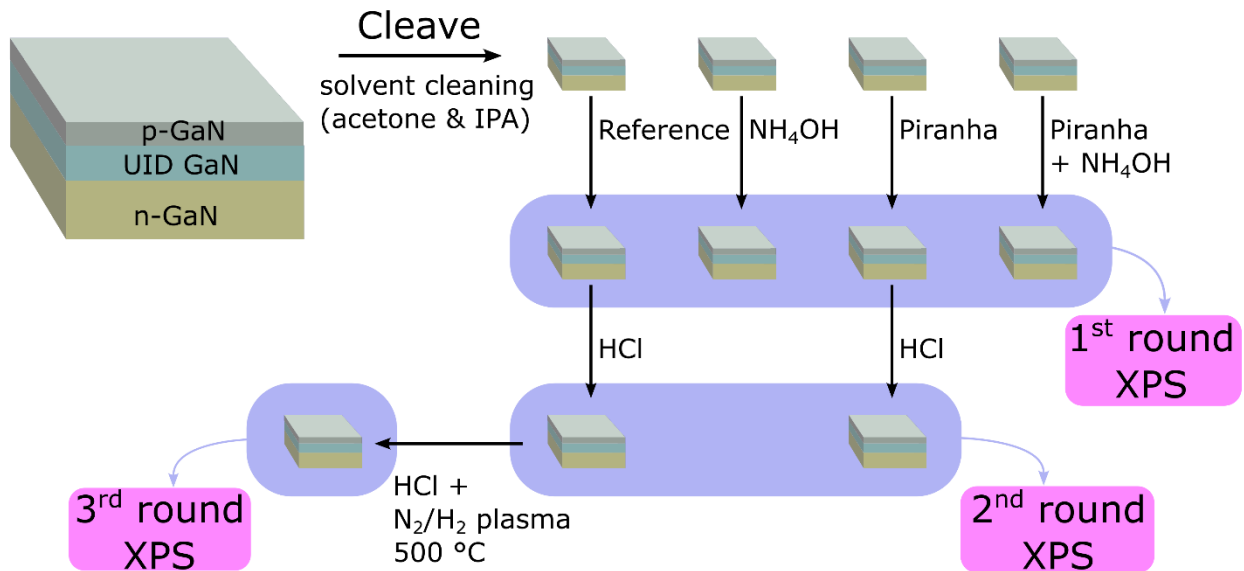


Figure 1. Overview of cleaning procedures and measurement flow.

2.3 Photoelectron characterization

XPS was measured at normal emission in a commercial system with a hemispherical analyzer. The base pressure was 6×10^{-9} mbar (6×10^{-7} Pa) or lower. Spectra were measured using monochromatic Al K α excitation (10 mA, 15 kV) with a pass energy of 20 eV (for high resolution spectra) or 160 eV (for survey spectra), step size of 0.1 eV (for high resolution

spectra) or 0.5 eV (for survey spectra), and a nominal analysis area of 1 mm². The binding energy was calibrated by measuring the core level energy of sputter cleaned noble metals²⁷ and no charge compensation was used.

The relative sensitivity factor, photoelectron inelastic mean free path, and transmission function were accounted for when analyzing and comparing the integrated areas of different core levels.

The thickness of surface layers was estimated using the method developed by Hill et al.^{28,29}

$$t = \lambda \cos\theta \ln \left(1 + \frac{I_o/S_o}{I_s/S_s} \right) (1)$$

where t is the overlayer thickness, λ is the photoelectron attenuation length, θ is the emission angle ($\theta = 0$ for normal emission), I_o and I_s are the core level peak intensities of the overlayer and substrate, respectively, and S_o and S_s are the core level sensitivity factors for the overlayer and substrate, respectively. The Ga 2p_{3/2} core level was used as the substrate core level for estimating the carbon and oxygen overlayer thicknesses, while the Ga 3s core level was used when calculating the Cl and S thicknesses.

The Ga 2p_{3/2} core levels were fit with a Voigt function³⁰ with a fixed full width at half maximum (1.9 eV) and a Shirley background to extract the contributions from the Ga-O and Ga-N binding states. The position of the Ga-O state was fixed at 1.3 eV higher binding energy than the Ga-N state³¹.

The PEEM system used was described previously^{32,33}. The base pressure of the measurement chamber was better than 10⁻⁹ mbar (1×10⁻⁷ Pa). GaN samples were outgassed at 500 K overnight before measurements. The light source was a conventional 100 W high-pressure Hg lamp. PEEM images were taken at room temperature with a 50 μm field of view and no beam-restricting apertures. The image of the as-received GaN was taken with a 10 s camera exposure time, 30 averages, and a detector voltage of 1340 V. The image of the HCl and plasma-cleaned GaN was taken with a 5 s camera exposure time, 50 averages, and a detector voltage of 1400 V. Images were corrected for detector non-uniformity using a standard flat-field and dark image method. Sample position drift was corrected before averaging individual frames. Images were corrected for different camera exposure times and detector voltages to allow for a direct comparison of the photoemission intensity.

3. RESULTS

3.1 Contamination reduction

Following the experimental flow illustrated in Figure 1, XPS spectra were recorded after the various cleaning methods to assess their efficacy. We first show the survey spectra in Figure 2a, where the main core level peaks associated with GaN (e.g., Ga 2p, N 1s, Ga 3d, and Ga LMM) and atmospheric contaminants (O 1s and C 1s) are observed for all samples. The integrated areas of the O 1s and C 1s core levels, relative to the Ga 2p_{3/2} core level, are compared in Figure 2b, along with the ratio between the Ga 2p_{3/2} and Ga 3d_{5/2} core levels.

From the changes in the C 1s core levels, we find that treatments using piranha reduced the carbon surface contaminants from a thickness of approximately 1.6 nm ± 0.1 nm (reference) to roughly 0.56 nm ± 0.04 nm, where the error is the standard deviation from measurements at multiple locations on the sample. Treatments only using NH₄OH or HCl did not significantly change the amount of carbon contamination (1.4 nm ± 0.1 nm and 1.5 nm ± 0.1 nm, respectively). The plasma treatment reduced the carbon contamination by a similar amount as the piranha treatments (0.52 nm ± 0.01 nm). Conversely, NH₄OH and HCl treatments had larger effects on reducing the surface oxygen content. The estimated oxide thickness decreased from approximately 1.14 nm ± 0.01 nm for the reference sample to approximately 0.67 nm ± 0.04 nm and 0.66 nm ± 0.02 nm for the combined piranha + NH₄OH and piranha + HCl treatments, respectively. These changes are also correlated with the increase in the ratio of the more surface-sensitive Ga 2p_{3/2} core level to the bulk-sensitive Ga 3d_{5/2} level, indicating that surface contaminants are removed by the different treatments.

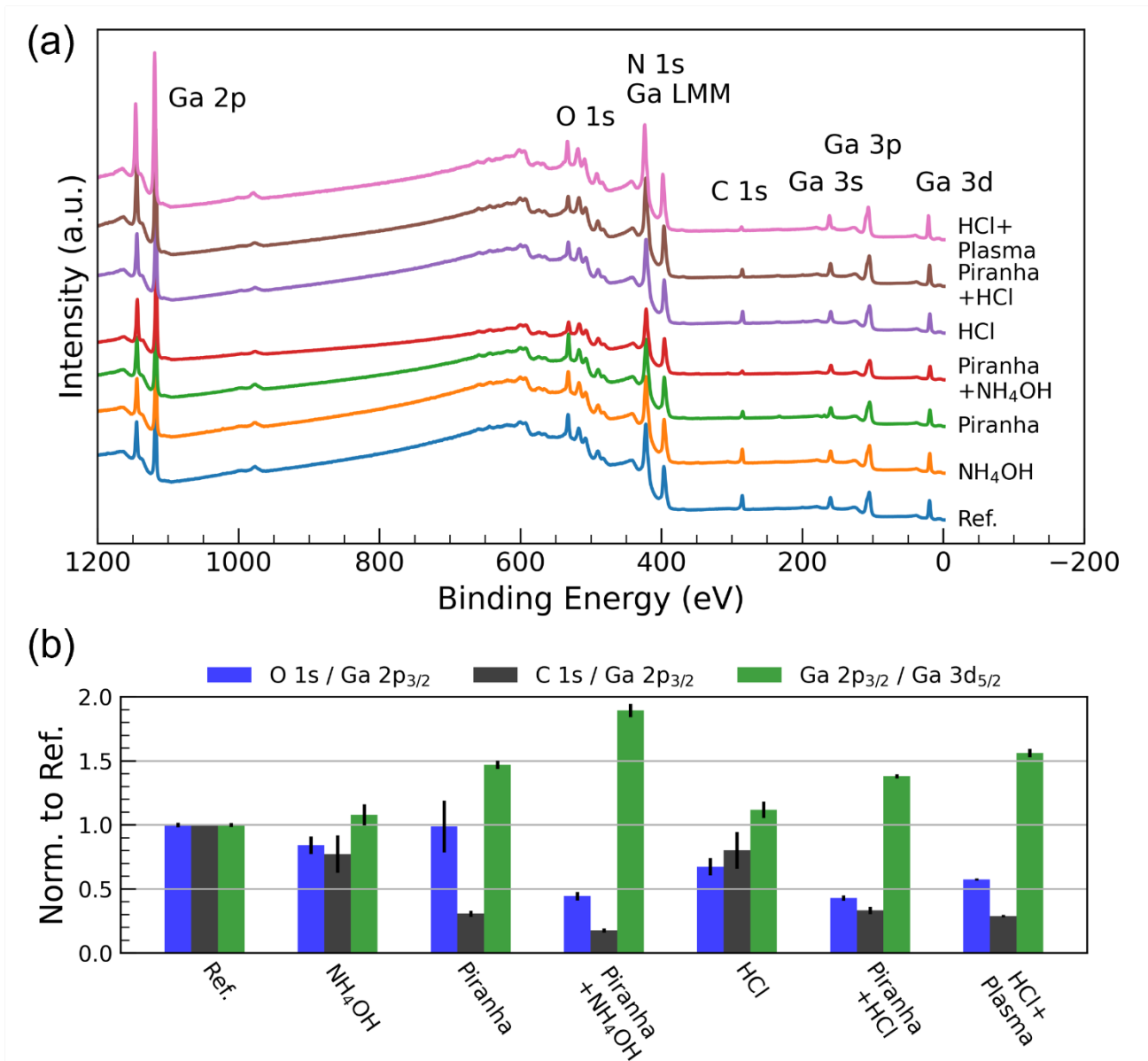


Figure 2. XPS survey of various cleaning methods. a) XPS survey spectra of the different cleaning methods, with the main core level contributions indicated. Spectra are offset for visibility. b) O 1s and C 1s area ratios relative to the Ga 2p_{3/2} core level and Ga 2p_{3/2} to Ga 3d_{5/2} ratio. The ratios are normalized to the reference sample for easier comparison. The error bars represent the standard deviation from measurements at different locations on the sample.

We now look in more detail at the Ga 2p_{3/2} core level following the different treatments, as shown in Figure 3a, where there are apparent changes in intensity and binding energy positions. The Ga 2p_{3/2} core level spectra were fit to extract the relative contributions of the Ga-O and Ga-N bonding states. A representative fit is shown for the reference sample in Figure 3a. The integrated area ratios of Ga-O to Ga-N from the Ga 2p_{3/2} core level are summarized in Figure 3b. The NH₄OH and HCl based treatments (except with plasma) have the largest reduction in the Ga-O contribution, which qualitatively agrees with the relative reduction in the integrated O 1s core level (Figure 2b).

Taking these results together, we conclude that combined ex-situ chemical cleaning treatments using piranha and either NH₄OH or HCl appear to have the largest effect of reducing the surface carbon and oxygen contamination levels on GaN. While the plasma treatment also successfully reduces the surface contamination, it causes large binding energy shifts,

which will be discussed in more detail in section 3.2. However, the oxygen and carbon removal is incomplete, in agreement with other reports in the literature using chemical cleaning methods²¹⁻²⁵. Hence, further in-situ cleaning is required to achieve pristine GaN surfaces. Therefore, for more detailed studies, combinations of treatments should be pursued to achieve the cleanest surface, e.g., ex-situ chemical cleaning followed by in-situ annealing and other treatments.

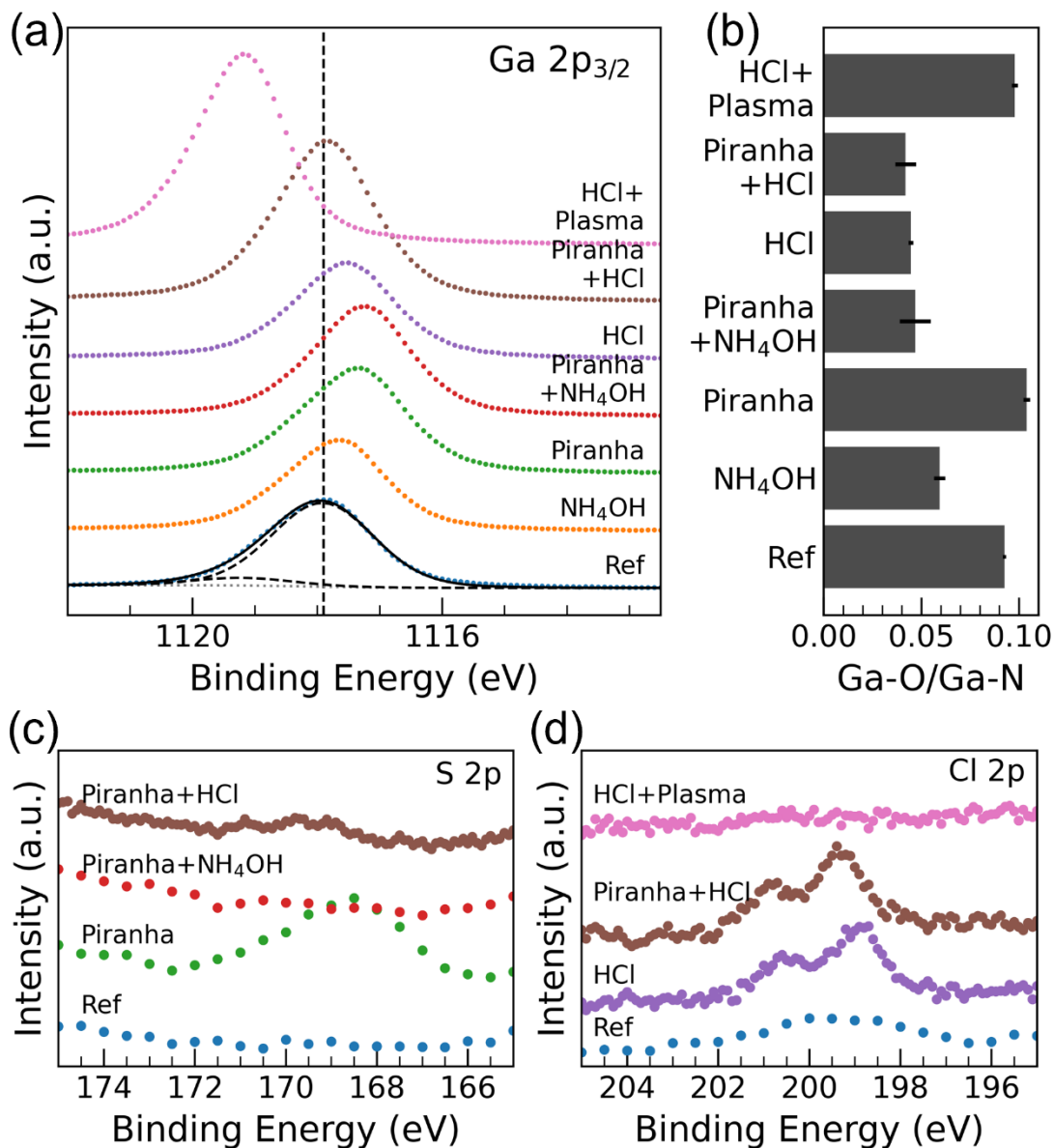


Figure 3. Detailed XPS core levels for the various cleaning methods. All spectra are offset for visibility. a) Ga 2p_{3/2} core levels. The dashed vertical line is a guide to the eye. The black dashed lines are fits of the Ga-O and Ga-N contributions (shown only for the Ref data in blue, for simplicity). The fitting background is represented by the grey dotted line, and the black solid line is the total fit. b) Ratio of the Ga-O area contribution to the Ga-N component of the Ga 2p_{3/2} core level for different treatments. The error bars represent the standard deviation of measurements at different locations on the sample. c) S 2p core level for different piranha treatments. d) Cl 2p core level for different HCl treatments.

Aside from the main core levels, we also observe binding states related to sulfur (Figure 3c) and chlorine (Figure 3d) following piranha and HCl treatments, respectively. The S 2p core level at 169 eV binding energy, as shown in Figure 3c,

is visible for the sample treated only with piranha, and corresponds to a sulfate or metal sulfate bond³⁴. The resulting sulfur coverage is approximately 0.2 nm thick. Subsequent treatment with NH₄OH completely removes the S 2p signal, while subsequent treatment with HCl greatly reduces the S 2p core level intensity. Therefore, the sulfate is easily displaced by other treatments.

The Cl 2p core level with its spin-orbit splitting of 1.6 eV is clearly visible after treatment with HCl (Figure 3d) at a binding energy of 199 eV for the Cl 2p_{3/2} peak. Only one pair of peaks consistent with metal chloride is observed²⁴, indicating there is negligible organic chlorine. The coverage corresponds to approximately 0.4 nm of Cl. Pre-treatment with piranha does not appreciably change the Cl chemical state; however, the Cl 2p core level is not detectible after treatment with N₂/H₂ plasma at 773 K. This coincides with reports on the desorption of Cl from GaN at elevated temperatures^{21,25}.

These results provide further evidence to observations of passivation by S and Cl^{21,22,25,35–37}. Hence, HCl and H₂SO₄ based treatments can provide anion bonding or physisorption, which may be beneficial for short term passivation of GaN surfaces between processing steps. However, the removal process should then be considered in terms of the total processing procedure, as high temperatures or a reducing environment may be required to remove Cl.

3.2 Valence changes and electronic alignment

Here, we turn to the valence band region for a more detailed look at several of the treated surfaces to understand the electronic changes taking place at the surface. The Ga 3d core level spectra and valence band maximum (VBM) regions are shown in Figure 4a for different processing conditions and the Ga 3d peak center and extrapolated VBM positions are summarized in Figure 4b. Treatments that resulted in Ga 2p_{3/2} core level shifts to lower binding energy, such as piranha + NH₄OH, resulted in the same shifts for the Ga 3d and VBM positions. The dramatic change (≈ 1.6 eV) in core and valence levels with the plasma treatment compared to the reference can be attributed to the rapid uptake of H₂ at elevated temperatures, which de-activates the Mg dopant³⁸. Therefore, plasma cleaning of p-type (Mg doped) GaN may not be practical as a general cleaning method, unless the H₂ incorporation can be reliably eliminated. However, inducing semi-insulating GaN with plasma treatments has recently been explored as an alternative to ion implantation for high-voltage device isolation^{39,40}, which may have benefits due to less surface damage. Except for the plasma treatment, all ex-situ chemical cleaning methods shift the Ga core levels and VBM towards the Fermi level. Together, this shows that the different chemical treatments result in a more p-type surface, while the plasma treatment instead results in a more n-type surface. The surface VBM are shown for the reference sample, piranha + NH₄OH, and HCl + plasma treatments in Figure 4c and compared to the expected pristine GaN, where for heavily p-doped GaN, the VBM should be pinned by the Mg dopant level to approximately 0.3 eV²⁶. Thus, we can infer that our surface is not pristine p-GaN, and likely has a very thin native oxide remaining at the surface (as corroborated in Figure 2b) along with surface band bending.

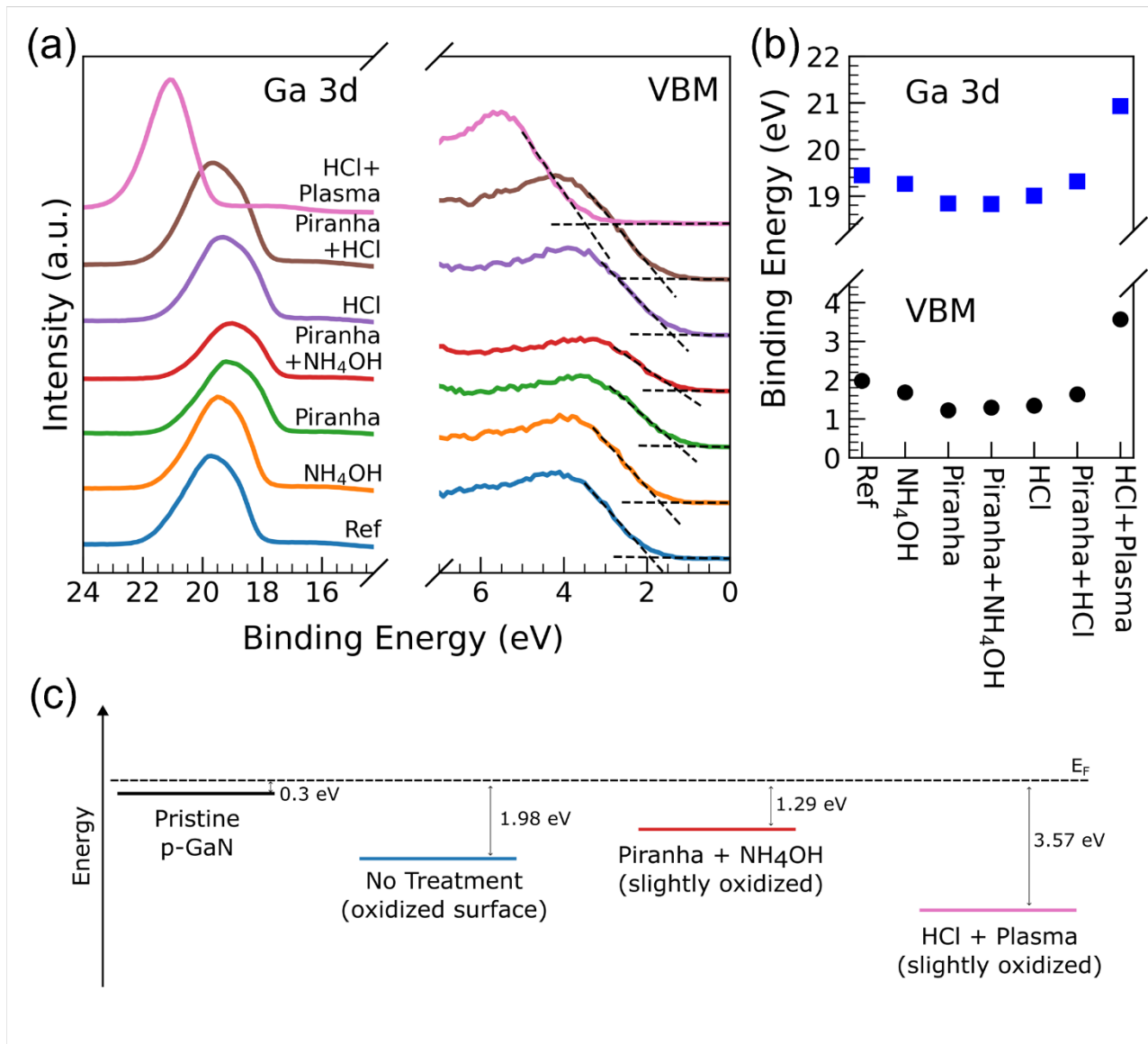


Figure 4. Determination of band alignment. a) XPS spectra of Ga 3d core level and valence band after different treatments. The spectra are offset vertically for visibility. The dashed lines are linear fits to extract the VBM. b) Extracted Ga 3d and VBM positions for the different treatments. c) Band alignment for the expected pristine p-GaN surface and measured VBM positions for the reference sample (no treatment), piranha + NH₄OH, and HCl + plasma treated samples with respect to the Fermi energy (E_F).

To further confirm the changes in valence structure from the plasma treatment, we also present PEEM images taken of an as-received sample stored in ambient after photoresist removal and the HCl + plasma treated sample (immediately after XPS measurements) using a Hg lamp as the UV light source. For the as-received sample shown in Figure 5a, there are surface features visible in the PEEM, such as bright smudges and spots scattered about on the sample, which are likely due to organic or adsorbate contamination. In contrast, the sample treated with HCl + plasma has considerably less photoemission intensity overall, as shown in Figure 5b. The HCl + plasma treated sample still exhibits some bright spots, though notably fewer and less intense. The reduction in photoemission intensity is quantified by the image histograms in Figure 5c, where the HCl + plasma treated sample has almost a tenth of the photoemission intensity of the sample from ambient. This agrees with the XPS results, where the valence band is much deeper for the HCl + plasma treated sample, resulting in considerably less threshold photoemission. However, for studying the GaN surface directly in PEEM, higher energy photons are needed, as evidenced by the long image exposure times needed using the conventional Hg lamp, despite

working at low magnifications. We are currently implementing a laser-based DUV setup to achieve photon energies up to 6.5 eV (compared to the maximum energy of 4.8 eV from the Hg lamp) with a high photon flux. This will enable advanced laboratory-based PEEM studies of the local electronic information around dislocations and other defects in GaN as a compliment to synchrotron-based studies⁴¹⁻⁴⁵.

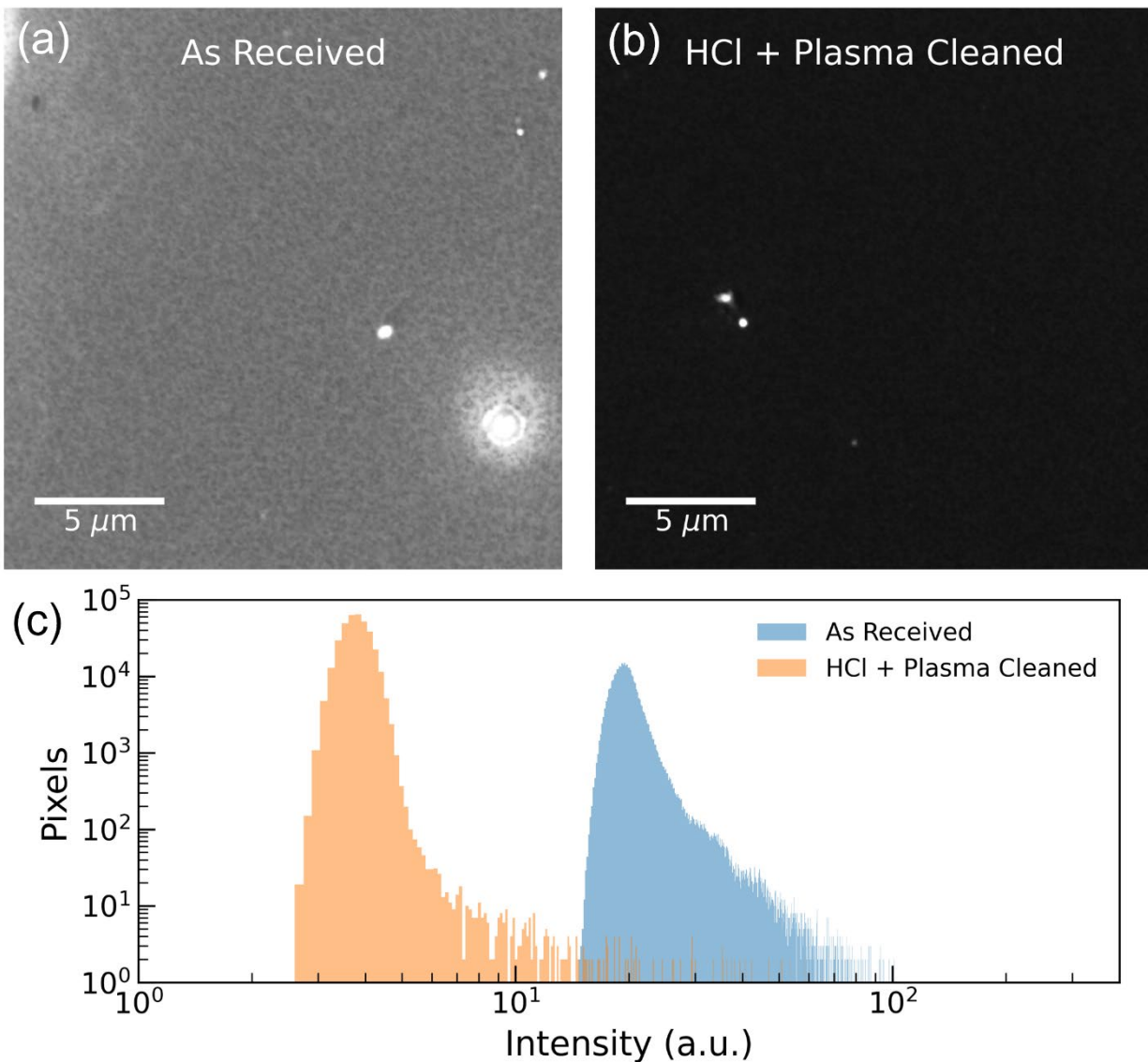


Figure 5. Threshold PEEM imaging. a) PEEM image of an as-received GaN surface after photoresist removal. b) PEEM image after cleaning with HCl and plasma. The images were corrected for different camera exposure conditions and are displayed on the same intensity range. c) Intensity histograms of the images shown in (a) and (b).

4. CONCLUSIONS

We have shown comparatively the results on extensive ex-situ chemical cleaning methods for GaN in preparation for PEEM experiments. We found that combined chemical treatments of piranha with either NH₄OH or HCl result in a reduction of the surface carbon and oxygen contamination. The reduction in contamination was correlated with shifts in the VBM to a more p-type surface. Initial PEEM results using a Hg lamp allow us to qualitatively evaluate surface contamination due to changes in threshold photoemission.

REFERENCES

1. Tsao, J. Y., Schubert, E. F., Fouquet, R. & Lave, M. The electrification of energy: Long-term trends and opportunities. *MRS Energy Sustain.* **5**, 5 (2018).
2. Tsao, J. Y. *et al.* Ultrawide-Bandgap Semiconductors: Research Opportunities and Challenges. *Adv. Electron. Mater.* **4**, 1600501 (2018).
3. Amano, H. *et al.* The 2018 GaN power electronics roadmap. *J. Phys. D: Appl. Phys.* **51**, 163001 (2018).
4. Parikh, P., Wu, Y. & Shen, L. Commercialization of high 600V GaN-on-silicon power HEMTs and diodes. in *2013 IEEE Energytech 1–5* (IEEE, 2013). doi:10.1109/EnergyTech.2013.6645300.
5. Parikh, P. *et al.* GaN Power Commercialization with Highest Quality-Highest Reliability 650V HEMTs-Requirements, Successes and Challenges. in *2018 IEEE International Electron Devices Meeting (IEDM) vols 2018-Decem 19.7.1-19.7.4* (IEEE, 2018).
6. Marzoughi, A., Romero, A., Burgos, R. & Boroyevich, D. Comparing the State-of-the-Art SiC MOSFETs: Test results reveal characteristics of four major manufacturers? 900-V and 1.2-kV SiC devices. *IEEE Power Electron. Mag.* **4**, 36–45 (2017).
7. Fu, H., Fu, K., Chowdhury, S., Palacios, T. & Zhao, Y. Vertical GaN Power Devices: Device Principles and Fabrication Technologies—Part I. *IEEE Trans. Electron Devices* **68**, 3200–3211 (2021).
8. Fu, H., Fu, K., Chowdhury, S., Palacios, T. & Zhao, Y. Vertical GaN Power Devices: Device Principles and Fabrication Technologies—Part II. *IEEE Trans. Electron Devices* **68**, 3200–3211 (2021).
9. Motoki, K. Development of gallium nitride substrates. *SEI Tech. Rev.* 28–35 (2010).
10. Key, D. *et al.* Structural and Electrical Characterization of 2” Ammonothermal Free-Standing GaN Wafers. Progress toward Pilot Production. *Materials (Basel)*. **12**, 1925 (2019).
11. Usami, S. *et al.* Correlation between dislocations and leakage current of p-n diodes on a free-standing GaN substrate. *Appl. Phys. Lett.* **112**, (2018).
12. Usami, S. *et al.* Correlation between nanopipes formed from screw dislocations during homoepitaxial growth by metal-organic vapor-phase epitaxy and reverse leakage current in vertical p–n diodes on a free-standing GaN substrates. *Jpn. J. Appl. Phys.* **58**, SCCB24 (2019).
13. Hite, J. K. *et al.* Effect of Surface Morphology on Diode Performance in Vertical GaN Schottky Diodes. *ECS J. Solid State Sci. Technol.* **6**, S3103–S3105 (2017).
14. Hite, J. K. *et al.* Influence of HVPE substrates on homoepitaxy of GaN grown by MOCVD. *J. Cryst. Growth* **498**, 352–356 (2018).
15. Gallagher, J. C. *et al.* Long range, non-destructive characterization of GaN substrates for power devices. *J. Cryst. Growth* **506**, 178–184 (2019).
16. Gallagher, J. C. *et al.* Effect of GaN Substrate Properties on Vertical GaN PiN Diode Electrical Performance. *J. Electron. Mater.* **50**, 3013–3021 (2021).
17. Gallagher, J. C. *et al.* Optimizing performance and yield of vertical GaN diodes using wafer scale optical techniques. *Sci. Rep.* **12**, 658 (2022).
18. Cao, Y., Pomeroy, J. W., Uren, M. J., Yang, F. & Kuball, M. Electric field mapping of wide-bandgap semiconductor devices at a submicrometre resolution. *Nat. Electron.* **4**, 478–485 (2021).
19. Narita, T. *et al.* Progress on and challenges of p-type formation for GaN power devices. *J. Appl. Phys.* **128**,

- 090901 (2020).
20. Fu, K. *et al.* The impact of interfacial Si contamination on GaN-on-GaN regrowth for high power vertical devices. *Appl. Phys. Lett.* **118**, 222104 (2021).
 21. Eller, B. S., Yang, J. & Nemanich, R. J. Electronic surface and dielectric interface states on GaN and AlGaIn. *J. Vac. Sci. Technol. A Vacuum, Surfaces, Film.* **31**, 050807 (2013).
 22. Bermudez, V. M. The fundamental surface science of wurtzite gallium nitride. *Surf. Sci. Rep.* **72**, 147–315 (2017).
 23. Liu, Z. *et al.* Optimization and characterization of III–V surface cleaning. *J. Vac. Sci. Technol. B Microelectron. Nanom. Struct.* **21**, 1953 (2003).
 24. English, C. R. *et al.* Impact of surface treatments on high- κ dielectric integration with Ga-polar and N-polar GaN. *J. Vac. Sci. Technol. B, Nanotechnol. Microelectron. Mater. Process. Meas. Phenom.* **32**, 03D106 (2014).
 25. Uhlrich, J. J., Grabow, L. C., Mavrikakis, M. & Kuech, T. F. Practical Surface Treatments and Surface Chemistry of n-Type and p-Type GaN. *J. Electron. Mater.* **37**, 439–447 (2008).
 26. Tracy, K. M., Mecouch, W. J., Davis, R. F. & Nemanich, R. J. Preparation and characterization of atomically clean, stoichiometric surfaces of n - and p -type GaN(0001). *J. Appl. Phys.* **94**, 3163–3172 (2003).
 27. International Organization for Standardization. Surface chemical analysis — X-ray photoelectron spectrometers — Calibration of energy scales (ISO Standard No. 15472:2010). <https://www.iso.org/standard/55796.html> (2010).
 28. Hill, J. M., Royce, D. G., Fadley, C. S., Wagner, L. F. & Grunthaner, F. J. Properties of oxidized silicon as determined by angular-dependent X-ray photoelectron spectroscopy. *Chem. Phys. Lett.* **44**, 225–231 (1976).
 29. Cumpson, P. J. The Thickogram: a method for easy film thickness measurement in XPS. *Surf. Interface Anal.* **29**, 403–406 (2000).
 30. CasaXPS LA(1.53,243) line shape.
 31. Wolter, S. D. *et al.* X-ray photoelectron spectroscopy and x-ray diffraction study of the thermal oxide on gallium nitride. *Appl. Phys. Lett.* **70**, 2156–2158 (1997).
 32. Niefind, F. *et al.* Imaging and measuring the electronic properties of epitaxial graphene with a photoemission electron microscope. *J. Appl. Phys.* **131**, 015303 (2022).
 33. Tromp, R. M. *et al.* A simple energy filter for low energy electron microscopy/photoelectron emission microscopy instruments. *J. Phys. Condens. Matter* **21**, 314007 (2009).
 34. NIST X-ray Photoelectron Spectroscopy Database, Version 4.1. <http://srdata.nist.gov/xps/> (2012).
 35. Huh, C., Kim, S. W., Kim, H. S., Lee, I. H. & Park, S. J. Effective sulfur passivation of an n-type GaN surface by an alcohol-based sulfide solution. *J. Appl. Phys.* **87**, 4591–4593 (2000).
 36. Martinez, G. L., Curiel, M. R., Skromme, B. J. & Molnar, R. J. Surface recombination and sulfide passivation of GaN. *J. Electron. Mater.* **29**, 325–331 (2000).
 37. Kerr, A. J. *et al.* Preparation of gallium nitride surfaces for atomic layer deposition of aluminum oxide. *J. Chem. Phys.* **141**, 104702 (2014).
 38. Jorg Neugebauer & Walle, C. G. Van de. Hydrogen in GaN: Novel Aspects of a Common Impurity. *Phys. Rev. Lett.* **75**, 252–255 (1995).
 39. Bian, Z., Zeng, K. & Chowdhury, S. 2.8 kV Avalanche in Vertical GaN PN Diode Utilizing Field Plate on Hydrogen Passivated P-Layer. *IEEE Electron Device Lett.* **43**, 596–599 (2022).
 40. Yang, C. *et al.* Low-leakage kV-class GaN vertical p–n diodes with non-destructive breakdown enabled by hydrogen-plasma termination with p-GaN extension. *Semicond. Sci. Technol.* **36**, 075009 (2021).
 41. Yang, W.-C., Rodriguez, B. J., Gruverman, A. & Nemanich, R. J. Photo electron emission microscopy of polarity-patterned materials. *J. Phys. Condens. Matter* **17**, S1415–S1426 (2005).
 42. Wu, C.-L., Lee, H.-M., Kuo, C.-T., Chen, C.-H. & Gwo, S. Cross-sectional scanning photoelectron microscopy and spectroscopy of wurtzite InN/GaN heterojunction: Measurement of “intrinsic” band lineup. *Appl. Phys. Lett.* **92**, 162106 (2008).
 43. Kuo, C. T., Lee, H. M., Shiu, H. W., Chen, C. H. & Gwo, S. Direct imaging of GaN p-n junction by cross-sectional scanning photoelectron microscopy and spectroscopy. *Appl. Phys. Lett.* **94**, 122110 (2009).
 44. Schmidt, T. H. *et al.* Mg and si dopant incorporation and segregation in gan. *Phys. Status Solidi Basic Res.* **248**, 1810–1821 (2011).
 45. Omika, K. *et al.* Operation Mechanism of GaN-based Transistors Elucidated by Element-Specific X-ray Nanospectroscopy. *Sci. Rep.* **8**, 13268 (2018).